symmetry

Article

Solitary Wave Propagation of the Generalized Rosenau–Kawahara–RLW Equation in Shallow Water Theory with Surface Tension

Akeel A. AL-saedi [1], Omid Nikan [2,*], Zakieh Avazzadeh [3,*] and António M. Lopes [4]

[1] Department of Mathematics, College of Education, Misan University, Misan 62001, Iraq; akeelmath@uomisan.edu.iq
[2] School of Mathematics and Computer Science, Iran University of Science and Technology, Tehran 16846-13114, Iran
[3] Department of Mathematical Sciences, University of South Africa, Florida 0003, South Africa
[4] LAETA/INEG, Faculty of Engineering, University of Porto, 4200-465 Porto, Portugal; aml@fe.up.pt
* Correspondence: omid_nikan@mathdep.iust.ac.ir (O.N.); avazzadz@unisa.ac.za (Z.A.)

Abstract: This paper addresses a numerical approach for computing the solitary wave solutions of the generalized Rosenau–Kawahara–RLW model established by coupling the generalized Rosenau–Kawahara and Rosenau–RLW equations. The solution of this model is accomplished by using the finite difference approach and the upwind local radial basis functions-finite difference. Firstly, the PDE is transformed into a nonlinear ODEs system by means of the radial kernels. Secondly, a high-order ODE solver is implemented for discretizing the system of nonlinear ODEs. The main advantage of this technique is its lack of need for linearization. The global collocation techniques impose a significant computational cost, which arises from calculating the dense system of algebraic equations. The proposed technique estimates differential operators on every stencil. As a result, it produces sparse differentiation matrices and reduces the computational burden. Numerical experiments indicate that the method is precise and efficient for long-time simulation.

Keywords: generalized Rosenau–Kawahara–RLW; solitary wave solutions; local meshless technique

check for updates

Citation: AL-saedi, A.A.; Nikan, O.; Avazzadeh, Z.; Lopes, A.M. Solitary Wave Propagation of the Generalized Rosenau–Kawahara–RLW Equation in Shallow Water Theory with Surface Tension. *Symmetry* **2023**, *15*, 1980. https://doi.org/10.3390/sym15111980

Academic Editor: Shou-Fu Tian

Received: 29 September 2023
Revised: 17 October 2023
Accepted: 23 October 2023
Published: 26 October 2023

1. Introduction

A disturbance of the ocean surface generally resulting from deep-sea earthquakes shifting the sea floor and generating tsunami waves and oceanic acoustic fields has interested scientists for a long time [1,2]. Tsunamis are near-shore propagating waves with long wavelengths and enormous amplitudes. The possibility of migration of these waves into the coast and devastation of property is substantial. Wave trains and wave forms with leading elevated or depressed waves have been previously observed. With respect to human catastrophes, the wavelength and amplitude ranges of these kinds of wave are considerable. Climate change and global warming are examples of these great natural disasters. Flooding, heat waves, early spring arrival, sea-level rise, glacier melting, coral reef bleaching, and disease contagions are the present-day results of climate change [3–7]. Nevertheless, these giant waves can constitute alternative energy resources for near-future applications if the essential technology is implemented [8–12].

Nonlinear partial differential equations (NPDEs) govern many natural phenomena arising in mathematical physics and engineering sciences [13–15]. Nonlinear waves are an important scientific research field. In recent decades, numerous scientists developed various mathematical models, such as the Korteweg–de Vries (KdV) [16], regularized-long wave (RLW) [17], and Rosenau [18] equations, to describe wave behavior. Indeed, the wave–wall and wave–wave interactions in compact discrete systems dynamics cannot be appropriately accomplished by the KdV model. To tackle this issue, Rosenau [19,20] introduced the following so-called Rosenau model:

$$u_t + u_{xxxxt} + u_x + uu_x = 0, \tag{1}$$

which commonly represents the dense discrete system and simulates the long-chain transmission model via an L-C flow in the computer and radio fields. The symbol $u = u(x,t)$ represents the wave velocity and the term $-u_{xxt}$ in the Rosenau model (1) is used to take into account nonlinear waves. Park [21] proved the uniqueness and existence of the solution to (1).

For further analysis of nonlinear waves, one term $-u_{xxt}$ needs to be involved in the Rosenau Equation (1). The obtained model is typically known as the following Rosenau–RLW model [22–24]:

$$u_t + u_{xxxxt} - u_{xxt} + uu_x + u_x = 0. \tag{2}$$

Following [25,26], the Rosenau–RLW model can be developed in the generalized Rosenau–RLW model as:

$$u_t - u_{xxt} + u_{xxxxt} + u_x + u^p u_x = 0, \tag{3}$$

in which $p \geq 1$ is a positive integer.

The KdV equation was modified by Kawahara [27] using solitary waves to balance the nonlinear effect via the higher-order dispersion effect. Hence, Kawahara [27] introduced a generalized non-linear dispersive relationship through the addition of a fifth-order term to this model. He took into account the effects of higher-order dispersion by approximating his model in the following form:

$$u_t + u_x + uu_x + u_{xxx} - u_{xxxxx} = 0. \tag{4}$$

The Kawahara-type equation was proposed for the shallow water wave theory with surface tension [27]. If the third nonlinear term on the left-hand side of the equation is substituted by $u^2 u_x$, then the Equation (4) is called as the modified Kawahara equation.

In order to take nonlinear waves into consideration, Pan and He [28] derived the Rosenau–Kawahara equation with the addition of the viscous terms $-u_{xxxxx}$ and $+u_{xxx}$ and obtained the generalized form of the Rosenau–RLW model (3). They investigated the solitary and periodic solutions of the following equation:

$$u_t + u_x + u^p u_x + u_{xxx} - u_{xxt} + u_{xxxxt} - u_{xxxxx} = 0. \tag{5}$$

In this paper, we focus on finding the approximate solutions of the initial boundary value problem (IBVP) for the one-dimensional (1D) generalized Rosenau–Kawahara–RLW model as

$$u_t + \alpha u_x + \beta u^p u_x + \gamma u_{xxx} - \mu u_{xxt} + \eta u_{xxxxt} - \sigma u_{xxxxx} = 0, \tag{6}$$

where the initial and boundary conditions (abbreviated as IC and BCs, respectively) are prescribed as

$$u(x,0) = g(x), \tag{7}$$
$$u(a,t) = u(b,t) = u_x(a,t) = u_x(b,t) = u_{xx}(a,t) = u_{xx}(b,t) = 0, \tag{8}$$

in which constants $\alpha, \beta, \gamma, \eta, \sigma$ and μ represent non-negative constants, $p \geq 2$ denotes a positive integer, $g(x)$ is prescribed continuous function, and $u = u(x,t)$ is a real-valued function.

When $\gamma = \sigma = 0$, Equation (6) converts to the generalized Rosenau–RLW model. For the case of $\alpha = \mu = \eta = 1$, $\gamma = \sigma = 0$ and $\beta = 2$, Equation (6) becomes to the usual Rosenau–RLW model. For the special case $\alpha = \gamma = \eta = \sigma = 1$, $\mu = 0$ and $\beta = 2$, Equation (6) corresponds to the usual Rosenau–Kawahara model and for $\mu = 0$, Equation (6) becomes the generalized Rosenau–Kawahara model.

Lemma 1 (See [28])**.** *Let $u_0(x) \in C_0^7([a,b])$. Then, the IBVP (6)–(8) satisfies the following energy conservative property:*

$$E(t) = \int_a^b (u^2 + \mu u_x^2 + \eta u_{xx}^2)\mathrm{d}x = ||u||_{L^2}^2 + \mu||u_x||_{L^2}^2 + \eta||u_{xx}||_{L^2}^2 = E(0), \quad \mu, \eta > 0,\ t \in [0, T],$$

where $C_0^7([a,b])$ represents the set of functions that are seventh order continuous differentiable in the spatial interval $[a,b]$ and have compact supports inside (a,b).

Over the last few years, some analytical and numerical approaches have been adopted to obtain the solution of the IBVP (6)–(8). Jin [29] applied the homotopy perturbation and variational iteration methods. Korkmaz and Dag [30] used the cosine expansion and Lagrange interpolation polynomials based on differential quadrature. Zuo [31] adopted the tanh ansatz and sech ansatz techniques to obtain exact bright and dark 1-soliton solutions. Pan and He [28] proposed a three-level linearly implicit finite difference (FD) approach. Later, He [32] derived the exact solitary wave solution with power law nonlinearity and advanced a three-level linearly implicit difference approach. Wang and Dai [33] developed a three-level conservative fourth-order FD approach, while Gazi et al. [34] employed a septic B-spline collocation finite element (FE) technique.

Mesh-free (meshless) methods have drawn considerable interest from the scientific community in recent decades. Unlike conventional mesh-dependent techniques (such as the FE, FD, and spectral techniques), these methods are independent of predefined grids and alignment for discretizing the domain. They use merely a group of scattered nodes provided by the initial data in order to cover the interior and the boundaries of the domain. They are also independent of the problem's geometry. The radial basis function (RBF) is one type of these methods. The RBF method utilizes a univariate function with an Euclidean norm, which converts a multidimensional problem into one that is virtually one-dimensional. Meshless RBFs have recently been widely utilized as a potential choice for solving PDEs in different applications [35]. The meshless characteristic of RBF-based methods provides flexibility with respect to the problem geometry, simplicity of multidimensional application, and a high convergence order. The RBF method may be either local or global, each of which has advantages and disadvantages. In global methods, all the nodal points in the domain of the problem are used, and implementation is simple. Small-scale problems can be easily solved by global methods, although ill-conditioned interpolation matrices are often encountered in these techniques. On the other hand, the local RBF techniques use only nodes in every subdomain's influence area around each spatial point. This mitigates the original ill-conditioning problem and the computational cost. Some authors have tried localized RBF-based strategies, such as the localized RBF-generated FD (LRBF-FD) [36,37] and the localized RBF partition of unity (LRBF-PU) [38,39], which produce well-conditioned systems.

The major objective of this work is to implement the meshfree LRBF-FD strategy for computing the solitary wave propagation of the generalized Rosenau–Kawahara–RLW model. The major advantages of the proposed mesh-free (meshless) technique and the related generalization over surfaces are that they are independent from a background mesh or cell for approximation and are easy to implement on different irregular domains in multi-dimensional spaces. The meshless LRBF-FD is the hybridization of the meshless concept with the FD technique. Nonetheless, this approach does not require meshing over the stencil nodes (the local subdomain or the subdomain), unlike the FD method. This process is performed for all grid points within the computational region. In addition, the grid points in each stencil can be readily increased for improving accuracy.

The outline of this paper has been organized as follows. Section 2 introduces the LRBF-FD strategy and the meshfree scheme of lines is applied to discretize the spatial variable of the generalized Rosenau–Kawahara–RLW model. Consequently, a nonlinear system of ODEs is derived that can be solved using either a numerical time stepping method or a direct solution in the time dimension. Some numerical tests are given in Section 3 to verify the numerical accuracy and performance of the LRBF-FD. In addition, it is shown that the computational efficiency of the proposed method is sufficiently superior to one exhibited by the other schemes in the existing literature. Finally, Section 4 presents the concluding remarks.

2. The RBF Collocation Scheme

Let $X = \{x_1, x_2, \ldots, x_N\} \subseteq \mathbb{R}^d$, be a finite set of scattered data interpolation in a bounded and closed domain containing with corresponding values f_i for $i = 1, 2, \ldots, N$.

2.1. The RBF Collocation Technique

Based on the Kansa method [35], the RBF interpolation method uses linear combinations of translations of one function ϕ of a single real variable. In 1D, the basic RBF interpolant for the solution $u(x)$ at discrete nodes takes the form

$$u(x) \approx s(x, \varepsilon) = \sum_{j=1}^{N} a_j \phi_j(x) = \sum_{j=1}^{N} a_j \phi(||x - x_j||), \tag{9}$$

where a_j are unknown constants and $\|.\|$ represents the Euclidian norm, x_j are centers that coincide with the collocation nodes $x_i \in \Omega$ and $\phi_j(x) = \phi(||x - x_j||)$ are radial basis functions:

$$s(x_i, \varepsilon) = f_i, \qquad i = 1, \ldots, N. \tag{10}$$

Imposing Equation (10) in (9) on $u(x)$ leads to a system of linear equations of the form

$$A_\phi \Lambda = f, \tag{11}$$

with

$$A_{\phi,ij} = \phi_j(x_i), \quad f = \begin{bmatrix} f_1 \\ f_2 \\ \vdots \\ f_N \end{bmatrix}, \quad \Lambda = \begin{bmatrix} a_1 \\ a_2 \\ \vdots \\ a_N \end{bmatrix}, \qquad i, j = 1, \ldots, N,$$

where the unknown vector Λ can be computed by making use of the collocation method.

2.2. The LRBF-FD Collocation Technique

The global RBF (GRBF) method requires all the grid nodes in the domain to estimate differential operators $\mathcal{L}$ at a node as the center. Indeed, all the grid points in the spatial interval must be considered in order to calculate the interpolation coefficient. Nevertheless, a larger and ill-conditioned linear system is generated in GRBF, which may lead to uncertain outcomes. In contrast, the local RBF method can be used only for the stencil (restricted points) on every center instead of the whole point domain. This method results in a linear system that is sparse and better-conditioned, while obtaining good reliability for ill-conditioned problems. The LRBF-FD estimates the linear differential operator $\mathcal{L}$ via the FD at each stencil. For every stencil, a small linear system must be solved with a conditionally positive definite (CPD) coefficient matrix. The LRBF-FD constitutes a generalization of the traditional FD technique that replaces the polynomial interpolation within a FD stencil with the RBF interpolation to compute the weighting coefficients.

Suppose that $\Omega \subset \mathbb{R}$ and $x_i \in \mathbb{R}$ are arbitrary in which this node has a support domain with n_i points $I_i = \{x_{i_1}, x_{i_2}, \ldots, x_{i_{n_i}}\}$ inside its stencil. The FD scheme approximates the differential operator $\mathcal{L}$ at a reference node by using the weighted linear sum of function values at all grid nodes into its stencil, in which the weighting coefficients at the stencil can be achieved as comes next:

$$\mathcal{L}\, u(x_i) = \sum_{j=1}^{n_i} w_j u(x_{i_j}). \tag{12}$$

Figure 1 displays demonstration of the distributed points in the computational domain with a stencil at point x_3.

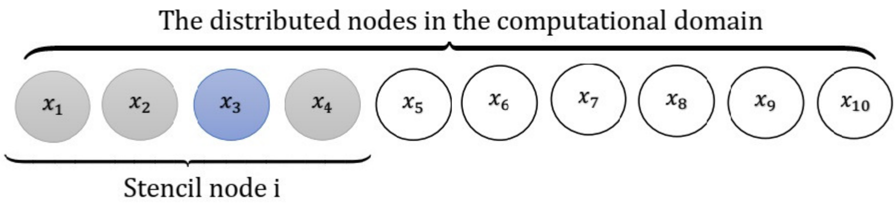

Figure 1. Demonstration of the distributed points in the computational region with a stencil at nodal point x_3.

The LRBF-FD computes the weighting coefficients $w_1, w_2, \ldots, w_{n_i}$ by enforcing the requirement that the linear combination (12) must be exact for the set of RBF, $\{\phi_j(x)\}\Big|_{j=1}^{n_i}$, where the centers are located at

$$\mathcal{L}\, u(x_i) = \sum_{j=1}^{n_i} w_j \phi_j(x_{i_j}). \tag{13}$$

In a more concise form, the LRBF-FD weights in (13) can be illustrated in a matrix form as

$$A_\phi\, w = \Psi\,, \tag{14}$$

where

$$w = \begin{bmatrix} w_1 \\ w_2 \\ \vdots \\ w_{n_i} \end{bmatrix}, \Psi = \begin{bmatrix} \mathcal{L}\phi_{i_1}(x)|_{x=x_i} \\ \mathcal{L}\phi_{i_2}(x)|_{x=x_i} \\ \vdots \\ \mathcal{L}\phi_{i_{n_i}}(x)|_{x=x_i} \end{bmatrix}, \quad A_{\phi,rs} = \phi_{i_r}(x_{i_s}), \quad r,\, s = 1, \ldots, n_i. \tag{15}$$

The weighting coefficients $w_1, w_2, \ldots, w_{n_i}$ are the unknown coefficients to be computed from the above-mentioned system at every stencil [40].

2.3. Discretization of the Generalized Rosenau–Kawahara–RLW Model

The LRBF-FD method approximates the unknown function by implementing RBFs while estimating the l^{th} derivative via the FD method. The major benefit of these methods is their approximation of derivatives using the FD scheme at every local support domain. As such, at each support domain, a small linear algebraic equations system must be resolved using the CPD interpolation matrix.

Here, we discretize spatial derivatives of the generalized Rosenau–Kawahara–RLW model by means of the LRBF-FD technique. Based on this, the first, third, fourth and fifth order derivatives of $u(x,t)$ can be approximated by means of the function values at all nodes in the stencil of x_i, as comes next:

$$u_x(x_i,t) = \sum_{j=1}^{n_i} w_{i,j}^{x,1} u(x_{i_j},t) = \mathbf{W}_x \mathbf{u}(t), \tag{16}$$

$$u_{xx}(x_i,t) = \sum_{j=1}^{n_i} w_{i,j}^{x,2} u(x_{i_j},t) = \mathbf{W}_{xx} \mathbf{u}(t), \tag{17}$$

$$u_{xxx}(x_i,t) = \sum_{j=1}^{n_i} w_{i,j}^{x,3} u(x_{i_j},t) = \mathbf{W}_{xxx} \mathbf{u}(t), \tag{18}$$

$$u_{xxxx}(x_i,t) = \sum_{j=1}^{n_i} w_{i,j}^{x,4} u(x_{i_j},t) = \mathbf{W}_{xxxx} \mathbf{u}(t), \tag{19}$$

$$u_{xxxxx}(x_i,t) = \sum_{j=1}^{n_i} w_{i,j}^{x,5} u(x_{i_j},t) = \mathbf{W}_{xxxxx} \mathbf{u}(t), \tag{20}$$

where the symbol $w_{i,j}^{x,l}$ denotes the weighted differences for the order derivatives $l = \{1,2,3,4,5\}$ and $\mathbf{u}(t) = [u_1(t),\ldots,u_N(t)]$ at every stencil. The matrices structure $\mathbf{W}_x$, $\mathbf{W}_{xx}$, $\mathbf{W}_{xxx}$, $\mathbf{W}_{xxxx}$ and $\mathbf{W}_{xxxxx}$ relies on the number of nodes in every stencil. For example, if we select three nodes at every stencil, then the matrices $\mathbf{W}_x$,$\mathbf{W}_{xx}$, $\mathbf{W}_{xxx}$, $\mathbf{W}_{xxxx}$ and $\mathbf{W}_{xxxxx}$ are tridiagonal matrices.

We obtain the following ODEs system by replacing Equations (16)–(20) in (6) and collocating nodes in it by

$$\frac{\mathrm{d}(\mathbf{I} - \mu\mathbf{W}_{xx} + \eta\mathbf{W}_{xxxx})\mathbf{u}(t)}{\mathrm{d}t} = -\alpha\mathbf{W}_x\mathbf{u}(t) - \beta\mathbf{u}^p(t).*\mathbf{W}_x\mathbf{u}(t) - \gamma\mathbf{W}_{xxx}\mathbf{u}(t) + \sigma\mathbf{W}_{xxxxx}\mathbf{u}(t). \tag{21}$$

Here, an ODE solver is adopted for solving the system of ODEs (21) in the temporal direction. The method of lines is a method that utilizes FD in the time dimension to solve ODE problems. If all eigenvalues of the spatial discretization technique, scaled by the time step (δt), are within the stability region of the spatial operator approximating time, then this method is considered stable. Algorithm 1 outlines the steps for fully discretizing the 1D Rosenau–Kawahara–RLW model using this approach.

Algorithm 1: Full discretization of the generalized Rosenau–Kawahara–RLW model

Enter the required simulation parameters such as: N, n_i, δt, T, α, β, μ, η, γ and σ;
$t_{\text{step}} = [0 : \delta t : T]$;
Construct the differentiation matrices $\mathbf{W}_x$, $\mathbf{W}_{xx}$, $\mathbf{W}_{xxx}$, $\mathbf{W}_{xxxx}$ and $\mathbf{W}_{xxxxx}$;
Construct the coefficient matrix of the ODE obtained :
$\mathbf{M} = \mathbf{I} - \mu\mathbf{W}_{xx} + \eta\mathbf{W}_{xxxx}$;
Make the right-hand side of (21):
RHS $= @(t,u) \quad -\alpha\mathbf{W}_x\mathbf{u}(t) - \beta\mathbf{u}^p(t).*\mathbf{W}_{xxx}\mathbf{u}(t) + \gamma\mathbf{W}_{xxx}\mathbf{u}(t) + \sigma\mathbf{W}_{xxxxx}\mathbf{u}(t)$;
Enter the IC $u_0 = g(x)$;
Apply the BC;
To solve the ODE obtained, use the following command:
opt = odeset('RelTol', 2.3 × 10^{-14}, 'AbsTol', 1 × 10^{-13}, 'Mass', **M**);
$[t,u] =$ ode15s$(@(t,u)$ RHS$(t,u), t_{\text{step}}, u_0,$ opt$)$;
Calculate the absolute error.

3. Numerical Experiments

This section introduces three numerical examples on the generalized Rosenau–Kawahara–RLW model to measure the accuracy and the performance of the LRBF-FD technique. For this purpose, we calculate the L_∞, L_2, and L_{rms} norm errors as

$$L_\infty = \max_{1\le i\le N}|u_i - U_i|,$$
$$L_2 = \sqrt{\sum_{i=1}^{N}(u_i - U_i)^2},$$
$$L_{\mathrm{rms}} = \sqrt{\frac{\sum_{i=1}^{N}(u_i - U_i)^2}{N}}.$$

Here, U_i and u_i denote the numerical and exact solutions, respectively. The numerical examples use the multiquadric RBF (MQ) $\phi(r) = \sqrt{1+\varepsilon^2 r^2}$ as the basis function with a shape parameter ε. The accuracy and flatness of the function heavily depend on this parameter ε, but there is no agreement on the best value. The LRBF-FD method places great importance on the selection of ε. To determine the optimal shape parameter ε, we utilize Algorithm 2 from Sarra's method [41].

Algorithm 2: Optimal shape parameter [41].

$K_{\min}$, $K_{\max}$, $\varepsilon_{\mathrm{Increment}}$
Optimal Shape Parameter
function OptimalShapeParameter($K_{\min}$, $K_{\max}$)
$K = 1$ **while** $K < K_{\min}$ or $K > K_{\max}$ **do**
  Construct interpolation matrix $\mathbf{M}$;
  $[U, S, V] = \mathrm{svd}(\mathbf{M})$;
  $K = \frac{\sigma_{\max}}{\sigma_{\min}}$; **if** $K < K_{\min}$ **then**
    $\varepsilon = \varepsilon - \varepsilon_{\mathrm{Increment}}$
  else
    $\varepsilon = \varepsilon + \varepsilon_{\mathrm{Increment}}$
  return ε

The `MATLAB R2016a` environment on a Windows 10 desktop computer with 4 GB RAM was used for numerical computations. The `condest command` in `MATLAB` can be used to obtain the condition number (CN) of the coefficient matrix.

Example 1. *Let us study the generalized Rosenau–Kawahara–RLW model* (6) *associated with* $\alpha = \beta = \mu = \eta = \sigma = 1$ *and* $p = 2$ *on the space interval* $[-40, 200]$ *so that exact solitary wave solution is*

$$u(x,t) = \frac{3}{4}\frac{\sqrt{370} - 5\sqrt{10}}{\sqrt{5\sqrt{37} - 29}}\,\mathrm{sech}^2\left[\frac{\sqrt{\sqrt{37} - 5}}{4}\left(x - \frac{33 - 5\sqrt{37}}{5\sqrt{37} - 29}t\right)\right]. \tag{22}$$

Hereafter, we study this example based on the LRBF-FD collocation technique for different values of δt, N, n_i and T. Table 1 reports the errors of numerical solutions L_∞, L_2, and L_{rms} norms, CN and computational times (in seconds) at different values of stencil sizes n_i with $\delta t = 1/1000$ when $T = 2$. Table 2 compares the errors of numerical solutions using L_∞ and L_2 norms with techniques described in [28,33] when $T = 10$ by taking $\delta t = 0.005$. Table 3 compares the L_∞ and L_2 norm errors with methods introduced in [28,33] by various values of δt and N when $T = 40$. Based on comparisons in Tables 2 and 3, we can observe that the proposed strategy is slightly better than the techniques introduced in [28,33]. Table 4 lists the conservative invariant E over spatial interval $[-40, 200]$ at various total times T. It can be seen that the method is conservative perfectly (up to 5 decimals) for energy during the long-term time evolution of the solitary wave. Figure 2 shows the numerical solution and corresponding maximum norm errors when $\delta t = 1/1000$, $N = 600$ and $n_i = 581$ over spatial interval $[-40, 200]$. Figure 3 displays the long-time behavior of numerical solutions with $N = 500$, $n_i = 467$ and $\delta t = 1/1000$ at several total times $T \in \{0, 20, 30, 40, 60\}$ over spatial interval $[-40, 200]$. As seen in Figure 3, the single solitons move to the right-side with the preserved amplitude and shape. Finally, Figure 4 depicts the maximum norm errors L_∞ at various total times $T \in \{0, 20, 30, 40, 60\}$ with $N = 350$, $n_i = 321$ and $\delta t = 0.01$ over spatial interval $[-40, 200]$.

Table 1. Errors using L_∞, L_2, and L_{rms} norms, CN and computational times with $\delta t = 1/1000$ at various stencil sizes n_i over spatial interval $[-40, 200]$ for Example 1 when $T = 2$.

N	n_i	L_∞	L_2	L_{rms}	CN	CPU Times
600	295	1.3656×10^{-6}	3.7376×10^{-6}	1.5259×10^{-7}	1.3729×10^{4}	3.285035
600	341	1.3268×10^{-6}	3.6333×10^{-6}	1.4833×10^{-7}	1.3732×10^{4}	3.289796
600	427	1.3028×10^{-6}	3.5684×10^{-6}	1.4568×10^{-7}	1.3735×10^{4}	3.291074
600	451	1.2926×10^{-6}	3.5449×10^{-6}	1.4472×10^{-7}	1.3736×10^{4}	3.333106
600	591	7.6618×10^{-7}	2.1733×10^{-6}	8.8726×10^{-8}	5.4577×10^{4}	3.499641

Table 2. Comparison of errors using L_∞ and L_2 norms with $\delta t = 0.005$ over spatial interval $[-40, 200]$ for Example 1 when $T = 10$.

h	Method	ε	N	n_i	L_∞	L_2
0.8						
	LRBF-FD	0.23	300	175	1.114×10^{-6}	3.518×10^{-6}
	Ref. [33]	–	300	–	1.177×10^{-4}	3.279×10^{-4}
	Ref. [28]	–	300	–	1.032×10^{-1}	2.660×10^{-1}
0.4						
	LRBF-FD	0.62	600	587	1.125×10^{-6}	7.358×10^{-6}
	Ref. [33]	–	600	–	5.431×10^{-5}	1.187×10^{-4}
	Ref. [28]	–	600	–	2.570×10^{-2}	6.650×10^{-2}
0.2						
	LRBF-FD	0.749	1200	1153	1.037×10^{-6}	8.134×10^{-6}
	Ref. [33]	–	1200	–	4.686×10^{-5}	1.124×10^{-4}
	Ref. [28]	–	1200	–	6.460×10^{-3}	1.666×10^{-2}
0.1						
	LRBF-FD	1.749	2400	2251	4.098×10^{-7}	4.981×10^{-6}
	Ref. [33]	–	2400	–	4.634×10^{-5}	1.118×10^{-4}
	Ref. [28]	–	2400	–	1.631×10^{-3}	4.209×10^{-3}

Table 3. Errors using L_∞ and L_2 norms over spatial interval $[-40, 200]$ for Example 1 when $T = 40$.

N	δt	Method [33]		LRBF-FD	
		L_2	L_∞	L_2	L_∞
300	0.4	3.3196758×10^{0}	1.2567252×10^{0}	1.5078×10^{-4}	4.5268×10^{-5}
600	0.1	1.6009018×10^{-1}	6.2383859×10^{-2}	7.7671×10^{-5}	1.4522×10^{-5}
1200	0.025	9.8513233×10^{-3}	3.8451638×10^{-3}	6.1025×10^{-5}	9.6039×10^{-6}

Table 4. The conservative invariant E over spatial interval $[-40, 200]$ at several values of total times T for Example 1.

T	Method [33]	LRBF-FD	T	Method [28]	LRBF-FD
0	25.44743969249009	25.44116739376160	0.05	25.451405792697514	25.44116739121527
10	25.44743945612407	25.44116721399481	19.95	25.451405792697514	25.44116705761903
20	25.44743934987927	25.44116705606914	39.95	25.451405792447929	25.44116686770641
30	25.44743928843207	25.44116686591815	59.95	25.451405792214793	25.44116686770641
40	25.44743923198240	25.44116649829927	79.95	25.451405791920855	25.44116686770641
50	25.44743917723612	25.44116687547143	99.95	25.451405792207414	25.44116686770641

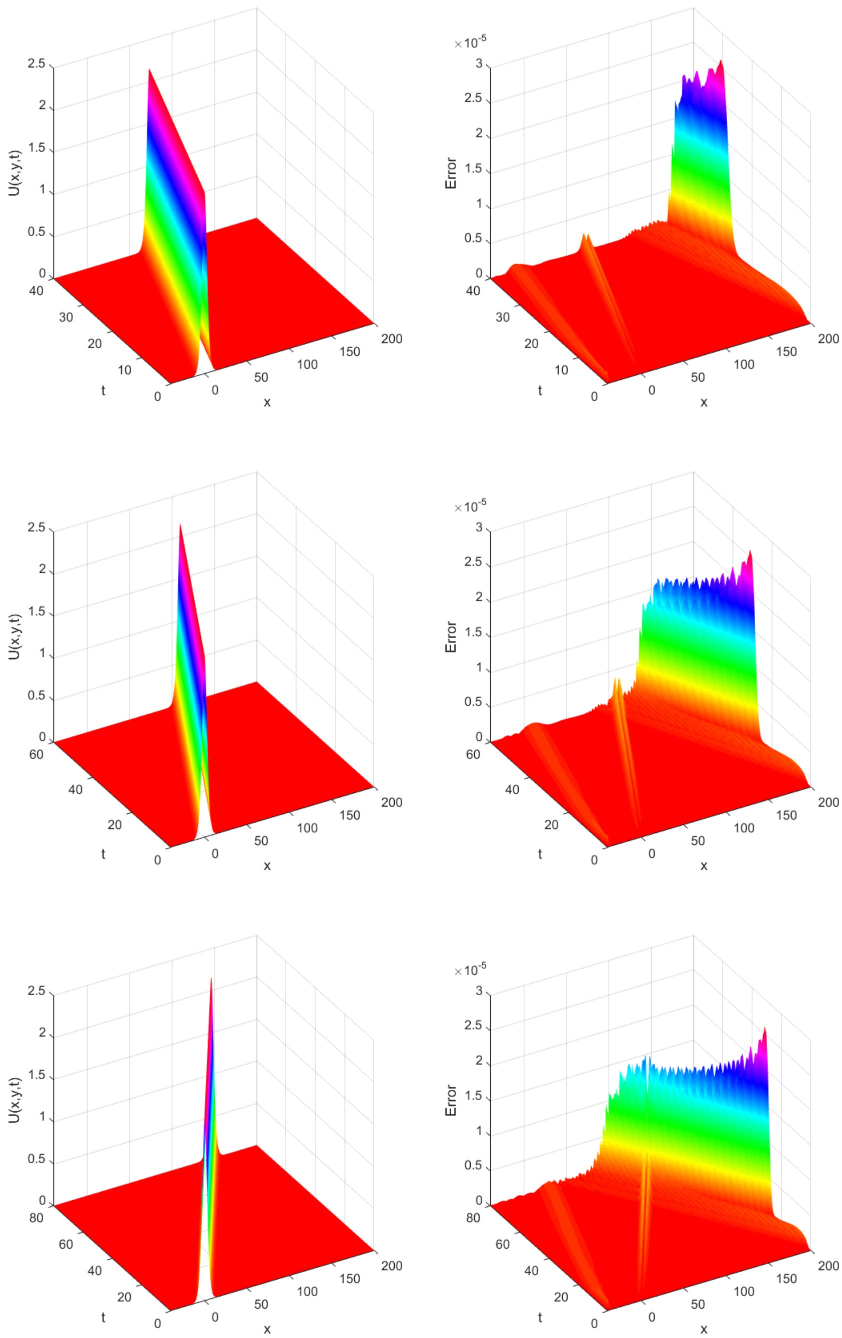

Figure 2. The approximation solution and corresponding maximum norm errors when $\delta t = 1/1000$, $N = 600$ and $n_i = 581$ over spatial interval $[-40, 200]$ for Example 1.

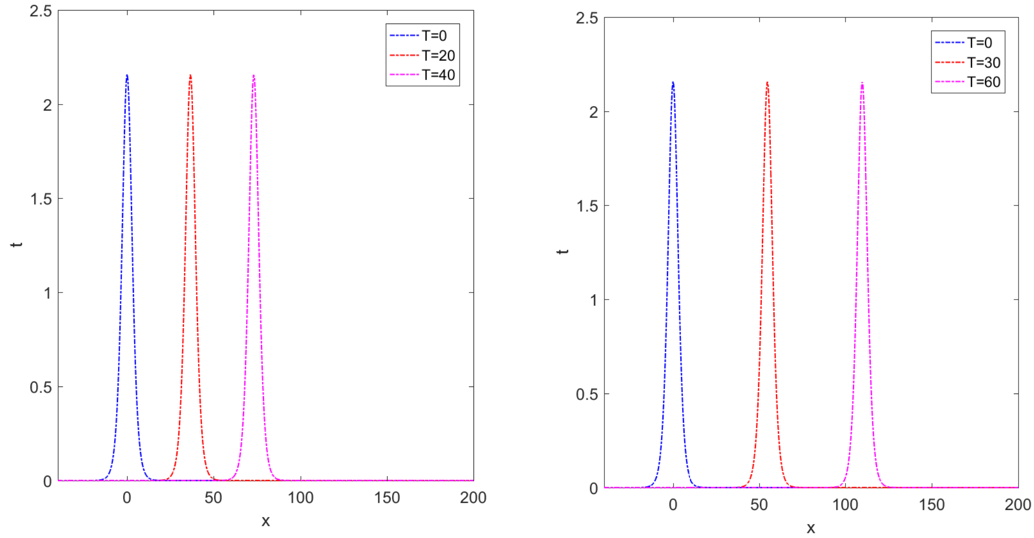

Figure 3. The long-time behavior of approximate solutions at various total times $T \in \{0, 20, 30, 40, 60\}$ with $N = 500$, $n_i = 467$ and $\delta t = 1/1000$ over spatial interval $[-40, 200]$ for Example 1.

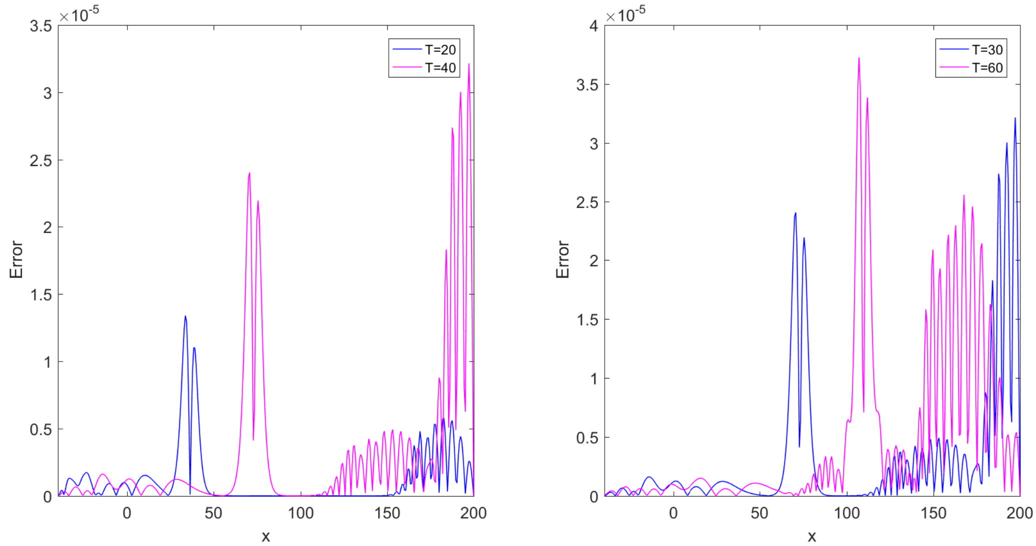

Figure 4. The maximum norm errors L_∞ at various total times $T \in \{0, 20, 30, 40, 60\}$ with $N = 350$, $n_i = 321$ and $\delta t = 0.01$ over spatial interval $[-40, 240]$ for Example 1.

Example 2. *Consider the generalized Rosenau–Kawahara–RLW model* (6) *associated with* $\alpha = \beta = \gamma = \eta = \sigma = 1$, $\mu = 2$ *and* $p = 4$ *on the space interval* $[-40, 240]$ *so that the exact solitary wave solution is*

$$u(x,t) = \left[\frac{40(\sqrt{127} - 10)^2}{3(10\sqrt{127} - 129)}\right]^{\frac{1}{4}} \operatorname{sech}\left[\frac{\sqrt{\sqrt{127} - 10}}{3}\left(x - \frac{118 - 10\sqrt{127}}{10\sqrt{127} - 109}t\right)\right]. \tag{23}$$

This example is simulated by using the LRBF-FD collocation scheme for different values of δt, N, n_i and T. Table 5 presents the errors of numerical solutions having L_∞, L_2, and L_{rms} norms, CN and computational times (in seconds) at several values of stencil sizes n_i with $\delta t = 1/1000$ when $T = 5$. Table 6 includes the errors of approximate solutions by making use of L_∞ and L_2 norms with techniques described in [28,33] by taking $\delta t = 0.005$ at total time $T = 10$. In view of Table 5, we can observe that the numerical accuracy of the LRBF-FD is clearly better than the technique described in [28,33]. Table 7 lists the conservative invariant E at several total times T over spatial interval $[-40, 240]$. One can observe that E is conserved (up to 8 decimals) and the method can be well applied to investigate the solitary wave over a long time. Figure 5 represents the long-time behavior of numerical solutions with $N = 500$, $n_i = 437$ and $\delta t = 1/1000$ at several total times $T \in \{0, 20, 30, 40, 60\}$ over spatial interval $[-40, 240]$. As observed in Figure 5, the single solitons move to the right side with the preserved amplitude and shape. Figure 6 shows the maximum norm errors L_∞ at several total times $T \in \{20, 30, 40, 60\}$ with $N = 1200$, $n_i = 1153$ and $\delta t = 0.1$ over spatial interval $[-40, 240]$. Figure 7 depicts the numerical solution and corresponding maximum norm errors L_∞ when $\delta t = 1/1000$, $N = 450$ and $n_i = 379$ over spatial interval $[-40, 240]$. Finally, Figure 8 depicts the relevant matrix's sparsity structures $\mathbf{M}$ with $N = 110$ in the case of $n_i \in \{11, 15\}$.

Table 5. Errors using L_∞, L_2, and L_{rms} norms, CN and computational times with $\delta t = 1/1000$ at various stencil sizes n_i over spatial interval $[-40, 240]$ for Example 2 when $T = 5$.

N	n_i	L_∞	L_2	L_{rms}	CN	CPU Times
700	341	1.7097×10^{-6}	8.8572×10^{-6}	3.3477×10^{-7}	1.8396×10^{4}	1.767428
700	457	1.5070×10^{-6}	6.5384×10^{-6}	2.4713×10^{-7}	1.8400×10^{4}	1.796425
700	571	1.4809×10^{-6}	6.0702×10^{-6}	2.2943×10^{-7}	1.3651×10^{4}	1.840518
700	677	1.4589×10^{-6}	5.1799×10^{-6}	2.1883×10^{-7}	1.3392×10^{4}	1.984204
700	695	1.4405×10^{-6}	5.1403×10^{-6}	1.9428×10^{-7}	1.8353×10^{5}	2.023724

Table 6. Errors using L_∞ and L_2 norms with $\delta t = 0.005$ at $T = 10$ over spatial interval $[-40, 240]$ for Example 2.

h	Method	ε	N	n_i	L_∞	L_2
0.8						
	LRBF-FD	0.23	300	175	1.815×10^{-6}	6.139×10^{-6}
	Ref. [33]	–	300	–	7.812×10^{-4}	1.684×10^{-3}
	Ref. [28]	–	300	–	5.839×10^{-2}	1.543×10^{-1}
0.4						
	LRBF-FD	0.62	600	587	1.823×10^{-6}	9.347×10^{-6}
	Ref. [33]	–	600	–	9.057×10^{-5}	2.037×10^{-4}
	Ref. [28]	–	600	–	1.446×10^{-2}	3.790×10^{-2}
0.2						
	LRBF-FD	0.749	1200	1153	1.545×10^{-6}	1.093×10^{-5}
	Ref. [33]	–	1200	–	3.270×10^{-5}	7.840×10^{-5}
	Ref. [28]	–	1200	–	3.599×10^{-3}	9.440×10^{-3}
0.1						
	LRBF-FD	1.749	2400	1541	1.190×10^{-6}	1.043×10^{-5}
	Ref. [33]	–	2400	–	2.890×10^{-5}	7.020×10^{-5}
	Ref. [28]	–	2400	–	9.011×10^{-4}	2.366×10^{-3}

Table 7. The conservative invariant E over spatial interval $[-40, 240]$ at various total times T for Example 2.

T	Method [33]	LRBF-FD	T	Method [28]	LRBF-FD
0	13.56376151273996	13.5545486917708	0.05	13.565665615099391	13.5545486917729
10	13.56376156073630	13.5545486910319	19.95	13.565665614771643	13.5545486904145
20	13.56376142914885	13.5545486904287	39.95	13.565665614965912	13.5545486914574
30	13.56376135010697	13.5545486912147	59.95	13.565665614937172	13.5545486900692
40	13.56376129439884	13.5545486914564	79.95	13.565665614960499	13.5545486949607
50	13.56376125125742	13.5545486907607	99.95	13.565665614998375	13.5545486936278

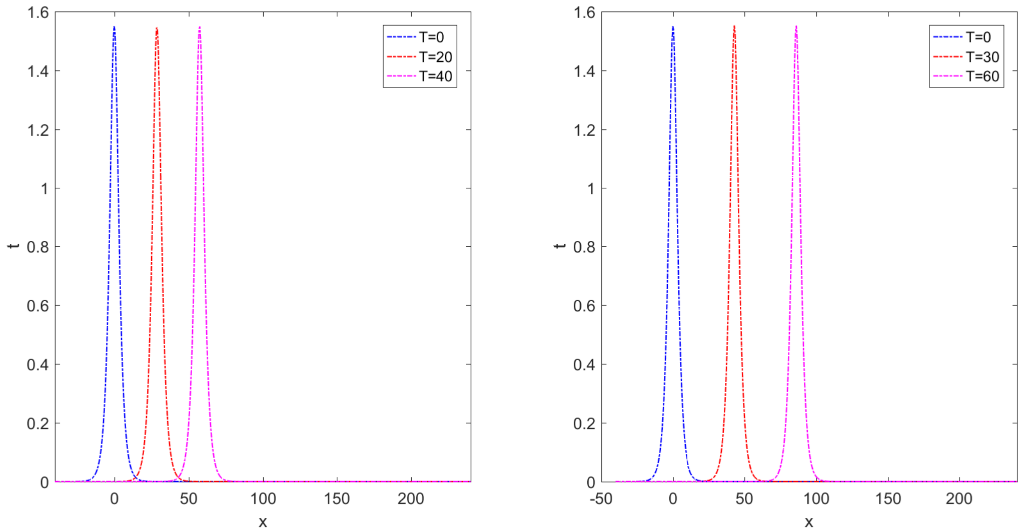

Figure 5. The long-time behavior of numerical solutions at several total times $T \in \{0, 20, 30, 40, 60\}$ with $N = 500$, $n_i = 437$ and $\delta t = 1/1000$ over spatial interval $[-40, 240]$ for Example 2.

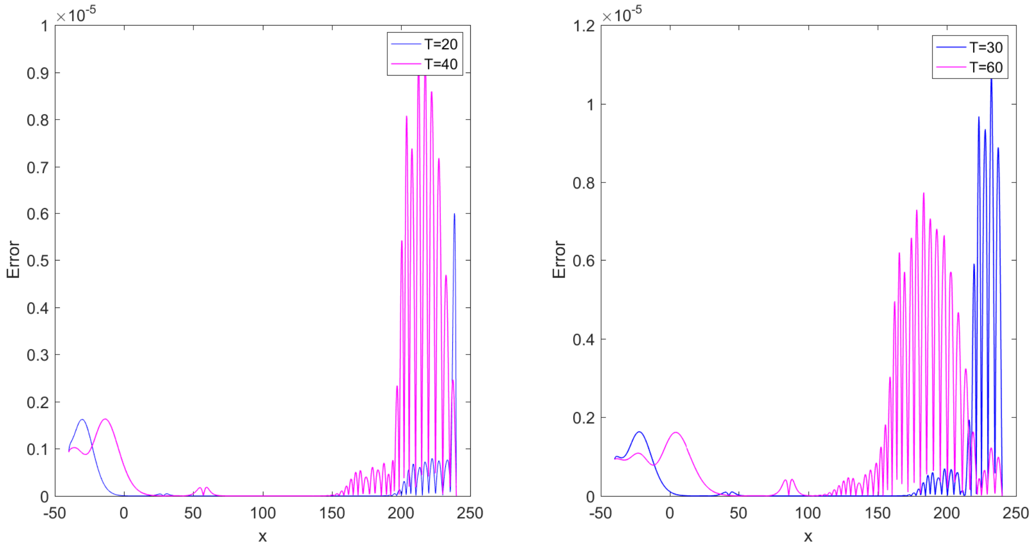

Figure 6. The maximum norm errors L_∞ at various total times $T \in \{20, 30, 40, 60\}$ with $N = 1200$, $n_i = 1153$ and $\delta t = 0.1$ over spatial interval $[-40, 240]$ for Example 2.

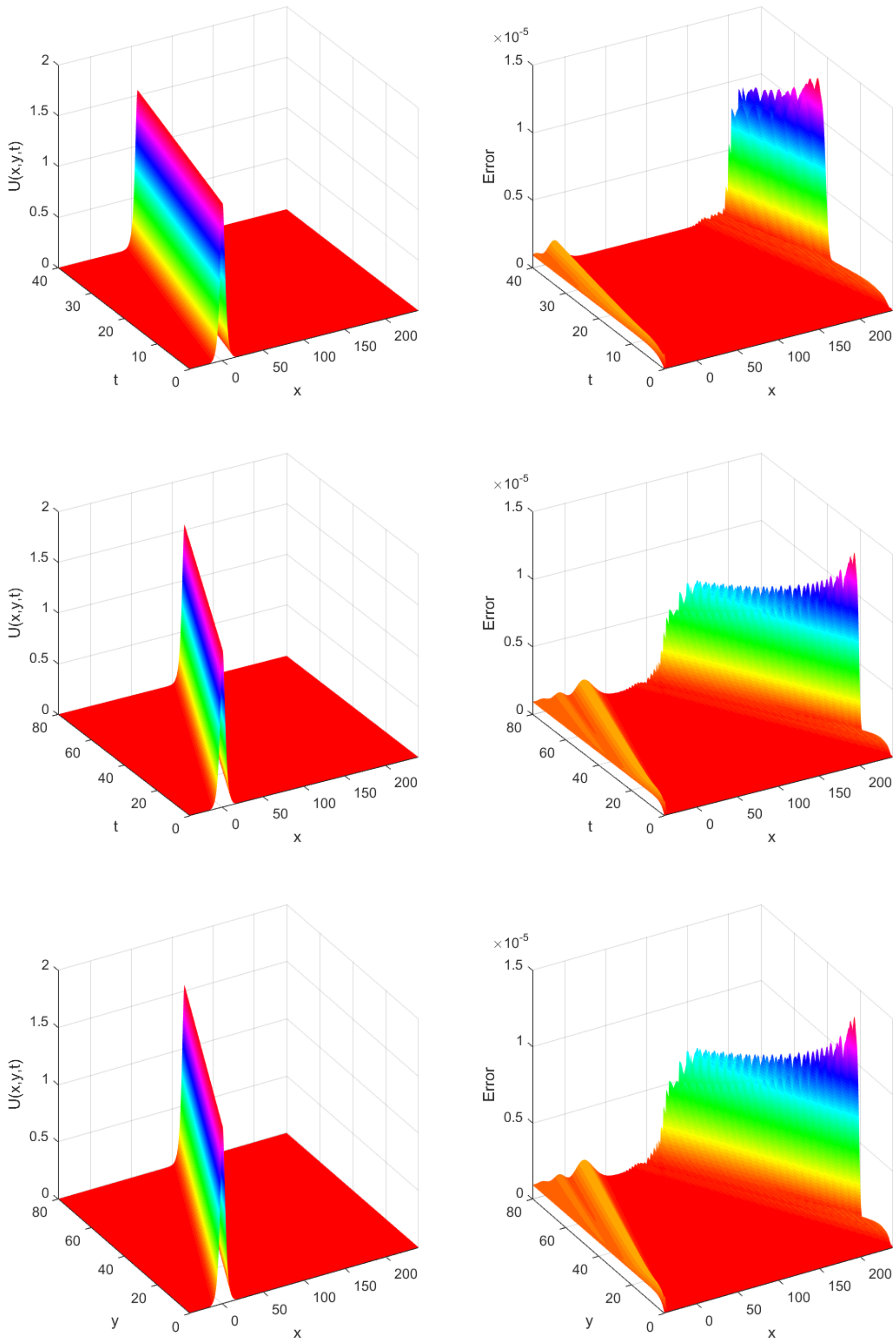

Figure 7. The approximation solution and corresponding maximum norm errors over spatial interval $[-40, 240]$ for Example 2 when $\delta t = 1/1000$, $N = 450$ and $n_i = 379$.

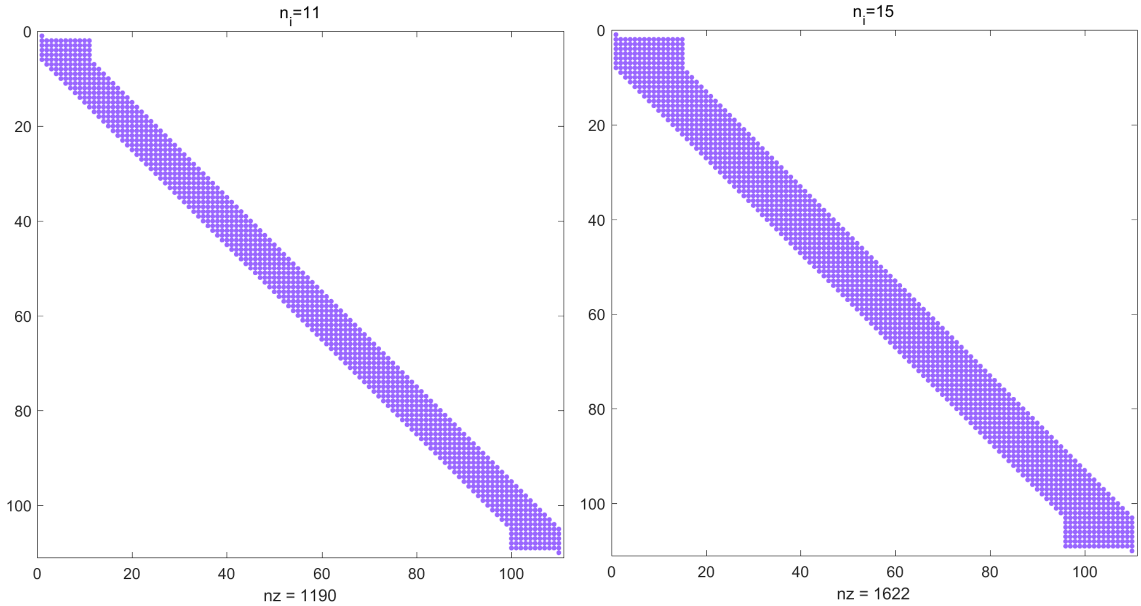

Figure 8. The sparsity structures of the relevant matrix $\mathbf{M}$ with $N = 110$ for $n_i \in \{11, 15\}$.

Example 3. *Consider the Kawahara-type Equation (6) with parameters as* $\alpha = \beta = \gamma = \sigma = 1$, $\eta = \mu = 0$ *and* $p = 1$ *on the space interval* $[-20, 30]$ *so that the exact solitary wave solution is*

$$u(x,t) = \frac{105}{169}\,\mathrm{sech}^4\left[\frac{\sqrt{13}}{26}\left(x - 2 - \frac{36}{169}t\right)\right]. \tag{24}$$

The LRBF-FD collocation method is adopted for solving this problem for different values of δt, N, n_i and T. Table 8 presents the errors of numerical solutions by means of L_∞, L_2 and $L_{\rm rms}$ norms, and computational times (in seconds) when $T = 1$ at several values of stencil sizes n_i with $\delta t = 0.01$. Table 9 represents the errors of approximate solutions based on L_∞ and L_2 norms with techniques described in [42,43] at several values of time step δt for $N = 250$, $n_i = 217$ and $c = 1.56$ over spatial interval $[-20, 30]$. In view of Table 8, we can see that the results by the proposed method show improvement over the techniques presented in [42,43]. Finally, Figure 9 depicts the numerical solution and corresponding maximum norm errors when $\delta t = 0.1$, $N = 250$ and $n_i = 235$ over spatial interval $[-20, 30]$.

Table 8. Errors using L_∞, L_2 and $L_{\rm rms}$ norms and CPU times with $\delta t = 1/1000$ when $T = 1$ and $N = 100$ at different stencil sizes n_i over spatial interval $[-20, 30]$ for Example 3.

n_i	L_∞	L_2	$L_{\rm rms}$	CPU Times
41	1.8552×10^{-2}	4.6501×10^{-2}	4.6501×10^{-3}	1.304175
55	1.5961×10^{-2}	3.9228×10^{-2}	3.9228×10^{-3}	1.308950
75	1.4311×10^{-3}	4.4648×10^{-3}	4.4648×10^{-4}	1.260047
79	1.4258×10^{-3}	4.4197×10^{-3}	4.4197×10^{-4}	1.313903
83	1.1660×10^{-3}	3.6052×10^{-3}	3.6052×10^{-4}	1.292554
87	7.6704×10^{-4}	2.3372×10^{-3}	2.3372×10^{-4}	1.323965
91	5.9984×10^{-4}	1.8503×10^{-3}	1.8503×10^{-4}	1.354920

Table 9. Errors using L_∞ and L_2 norms at several values of time step δt when $T = 1$, $N = 250$, and $n_i = 217$ over spatial interval $[-20, 30]$ for Example 3.

	$\delta t = 0.1$		$\delta t = 0.05$		$\delta t = 0.025$	
	L_∞	L_2	L_∞	L_2	L_∞	L_2
LRBF-FD	6.8953×10^{-6}	3.6243×10^{-5}	6.7890×10^{-6}	3.7916×10^{-5}	6.7890×10^{-6}	1.7916×10^{-5}
MQ-RBF [42]	3.7050×10^{-5}	7.5934×10^{-5}	2.1006×10^{-5}	4.3318×10^{-5}	1.1969×10^{-5}	2.8266×10^{-5}
MQ-RBF [43]	6.1666×10^{-3}	2.0797×10^{-3}	9.2686×10^{-4}	5.4222×10^{-4}	6.3848×10^{-4}	1.4557×10^{-4}
TPS-RBF [43]	2.0675×10^{-3}	8.7495×10^{-4}	1.0727×10^{-3}	4.5004×10^{-4}	7.4467×10^{-4}	2.6368×10^{-4}

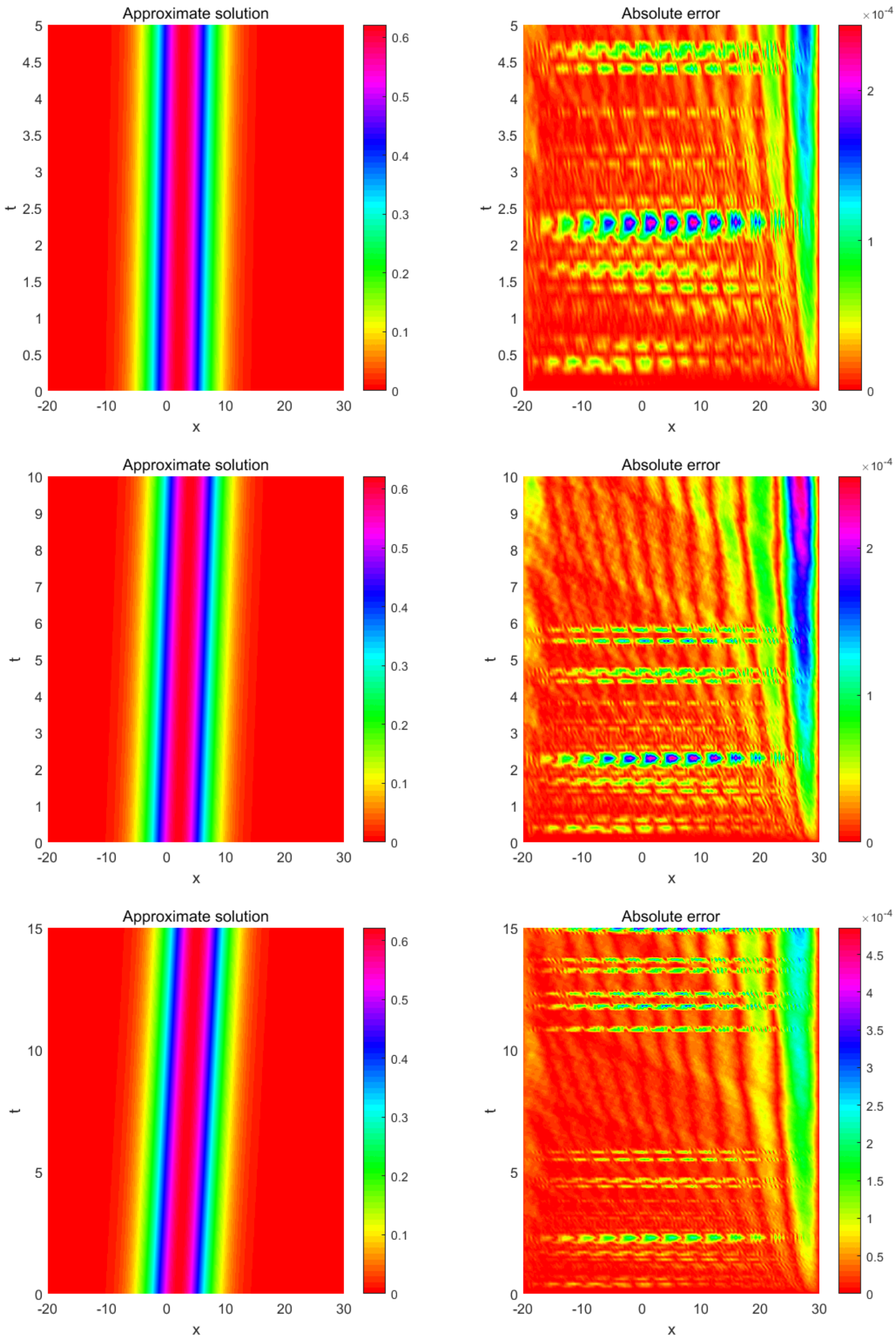

Figure 9. The approximation solution and corresponding maximum norm errors when $\delta t = 0.1$, $N = 250$ and $n_i = 235$ over spatial interval $[-20, 30]$ for Example 3.

4. Concluding Remark

This paper adopted a meshless numerical procedure for solving the IBVP of the generalized nonlinear Rosenau–Kawahara–RLW without using linearization. Firstly, the PDE was converted into a nonlinear system of ODEs through radial kernels. Afterwards, the method of lines was utilized to approximate the temporal direction and generate a system of nonlinear ODEs. Furthermore, an ODE solver was utilized to obtain highly accurate outcomes from the nonlinear ODEs system. Global RBF collocation techniques have the disadvantage of high computational cost and ill-conditioned system. The proposed method overcomes these challenges well and reduces the computational cost by sparsifying the linear system. Numerical results verified the reliability and efficiency of the present method when compared with existing ones.

Author Contributions: Conceptualization, A.A.A.-s. and O.N.; data curation, A.A.A.-s. and O.N.; formal analysis, O.N. and Z.A.; investigation, Z.A and O.N.; methodology, O.N. and Z.A.; software, O.N and Z.A.; supervision, Z.A. and A.M.L.; validation, O.N. and Z.A.; visualization, A.M.L. and O.N.; writing-original draft, Z.A. and O.N.; writing-review and editing, A.M.L. All authors have read and agreed to the published version of the manuscript.

Funding: This research received no external funding.

Data Availability Statement: No datasets were generated or analyzed during the current study.

Acknowledgments: The authors are thankful to the respected reviewers for their valuable comments and constructive suggestions towards the improvement of the original paper.

Conflicts of Interest: The authors declare no conflict of interest.

References

1. Chunga, K.; Toulkeridis, T. First evidence of paleo-tsunami deposits of a major historic event in Ecuador. *J. Tsunami Soc. Int.* **2014**, *33*, 69.
2. Smith, R.C.; Hill, J.; Collins, G.S.; Piggott, M.D.; Kramer, S.C.; Parkinson, S.D.; Wilson, C. Comparing approaches for numerical modelling of tsunami generation by deformable submarine slides. *Ocean Model.* **2016**, *100*, 125–140. [CrossRef]
3. Sakera, S.; Hassanb, H. Asymptotic properties of solutions of third-order nonlinear dynamic equations on time scales. *J. Math. Comput. Sci.* **2022**, *25*, 255–268. [CrossRef]
4. Ngondiep, E. A novel three-level time-split approach for solving two-dimensional nonlinear unsteady convection-diffusion-reaction equation. *J. Math. Comput. Sci* **2022**, *26*, 222–248. [CrossRef]
5. Kumar, P.; Panwar, V. Wavelet neural network based controller design for non-affine nonlinear systems. *J. Math. Comput. Sci.* **2022**, *24*, 49–58. [CrossRef]
6. Hussain, J. Exact solutions of transaction cost nonlinear models for illiq-uid markets. *J. Math. Comput. Sci.* **2021**, *23*, 263–278. [CrossRef]
7. Ibrahima, A.H.; Muangchoob, K.; Mohamedc, N.S.; Abubakard, A.B. Derivative-free SMR conjugate gradient method for con-straint nonlinear equations. *J. Math. Comput. Sci.* **2022**, *24*, 147–164. [CrossRef]
8. Hu, H. *Dynamics of Surface Waves in Coastal Waters*; Springer: Berlin/Heidelberg, Germany, 2010.
9. Pedlosky, J. *Waves in the Ocean and Atmosphere: Introduction to Wave Dynamics*; Springer: Berlin/Heidelberg, Germany, 2003; Volume 260.
10. Johnson, R.S. *A Modern Introduction to the Mathematical Theory of Water Waves*; Number 19; Cambridge University Press: Cambridge, UK, 1997.
11. Holthuijsen, L.H. *Waves in Oceanic and Coastal Waters*; Cambridge University Press: Cambridge, UK, 2010.
12. Barna, I.F.; Pocsai, M.A.; Mátyás, L. Time-dependent analytic solutions for water waves above sea of varying depths. *Mathematics* **2022**, *10*, 2311. [CrossRef]
13. Golbabai, A.; Arabshahi, M. On the behavior of high-order compact approximations in the one-dimensional sine—Gordon equation. *Phys. Scr.* **2011**, *83*, 015015. [CrossRef]
14. Molavi-Arabshahi, M.; Shavali-koohshoori, K. Application of cubic B-spline collocation method for reaction diffu-sion Fisher's equation. *Comput. Methods Differ. Equ.* **2021**, *9*, 22–35.
15. Khasi, M.; Rashidinia, J.; Rasoulizadeh, M.N. Fast Computing Approaches Based on a Bilinear Pseudo-Spectral Method for Nonlinear Acoustic Wave Equations. *SIAM J. Sci. Comput.* **2023**, *45*, B413–B439. [CrossRef]

16. Khan, K.; Akbar, M.A. Solving unsteady Korteweg–de Vries equation and its two alternatives. *Math. Methods Appl. Sci.* **2016**, *39*, 2752–2760. [CrossRef]
17. Rasoulizadeh, M.; Nikan, O.; Avazzadeh, Z. The impact of LRBF-FD on the solutions of the nonlinear regularized long wave equation. *Math. Sci.* **2021**, *15*, 365–376. [CrossRef]
18. Demirci, A.; Hasanoğlu, Y.; Muslu, G.M.; Özemir, C. On the Rosenau equation: Lie symmetries, periodic solutions and solitary wave dynamics. *Wave Motion* **2022**, *109*, 102848. [CrossRef]
19. Rosenau, P. A quasi-continuous description of a nonlinear transmission line. *Phys. Scr.* **1986**, *34*, 827. [CrossRef]
20. Rosenau, P. Dynamics of dense discrete systems: high order effects. *Prog. Theor. Phys.* **1988**, *79*, 1028–1042. [CrossRef]
21. Park, M. On the Rosenau equation. *Mat. Appl. Comput.* **1990**, *9*, 145–152.
22. Pan, X.; Zhang, L. On the convergence of a conservative numerical scheme for the usual Rosenau-RLW equation. *Appl. Math. Model.* **2012**, *36*, 3371–3378. [CrossRef]
23. Pan, X.; Zheng, K.; Zhang, L. Finite difference discretization of the Rosenau-RLW equation. *Appl. Anal.* **2013**, *92*, 2578–2589. [CrossRef]
24. Atouani, N.; Omrani, K. Galerkin finite element method for the Rosenau-RLW equation. *Comput. Math. Appl.* **2013**, *66*, 289–303. [CrossRef]
25. Zuo, J.M.; Zhang, Y.M.; Zhang, T.D.; Chang, F. A new conservative difference scheme for the general Rosenau-RLW equation. *Bound. Value Probl.* **2010**, *2010*, 1–13. [CrossRef]
26. Pan, X.; Zhang, L. Numerical simulation for general Rosenau-RLW equation: An average linearized conservative scheme. *Math. Probl. Eng.* **2012**, *2012*, 517818. [CrossRef]
27. Kawahara, T. Oscillatory solitary waves in dispersive media. *J. Phys. Soc. Jpn.* **1972**, *33*, 260–264. [CrossRef]
28. He, D.; Pan, K. A linearly implicit conservative difference scheme for the generalized Rosenau–Kawahara-RLW equation. *Appl. Math. Comput.* **2015**, *271*, 323–336. [CrossRef]
29. Jin, L. Application of variational iteration method and homotopy perturbation method to the modified Kawahara equation. *Math. Comput. Model.* **2009**, *49*, 573–578. [CrossRef]
30. Korkmaz, A.; Dağ, İ. Crank-Nicolson–differential quadrature algorithms for the Kawahara equation. *Chaos Solit. Fractals* **2009**, *42*, 65–73. [CrossRef]
31. Zuo, J.m. Soliton solutions of a general Rosenau-Kawahara-RLW equation. *J. Math. Res.* **2015**, *7*, 24. [CrossRef]
32. He, D. Exact solitary solution and a three-level linearly implicit conservative finite difference method for the generalized Rosenau–Kawahara-RLW equation with generalized Novikov type perturbation. *Nonlinear Dyn.* **2016**, *85*, 479–498. [CrossRef]
33. Wang, X.; Dai, W. A new implicit energy conservative difference scheme with fourth-order accuracy for the generalized Rosenau–Kawahara-RLW equation. *Comput. Appl. Math.* **2018**, *37*, 6560–6581. [CrossRef]
34. Gazi Karakoc, S.B.; Kumar Bhowmik, S.; Gao, F. A numerical study using finite element method for generalized Rosenau-Kawahara-RLW equation. *Comput. Methods Differ. Equ.* **2019**, *7*, 319–333.
35. Chen, W.; Fu, Z.J.; Chen, C.S. *Recent Advances in Radial Basis Function Collocation Methods*; Springer: Berlin/Heidelberg, Germany, 2014.
36. Avazzadeh, Z.; Nikan, O.; Machado, J.A.T. Solitary wave solutions of the generalized Rosenau-KdV-RLW equation. *Mathematics* **2020**, *8*, 1601. [CrossRef]
37. Nikan, O.; Avazzadeh, Z.; Machado, J.T. Numerical study of the nonlinear anomalous reaction–subdiffusion process arising in the electroanalytical chemistry. *J. Comput. Sci.* **2021**, *53*, 101394. [CrossRef]
38. Nikan, O.; Avazzadeh, Z.; Rasoulizadeh, M. Soliton wave solutions of nonlinear mathematical models in elastic rods and bistable surfaces. *Eng. Anal. Bound. Elem.* **2022**, *143*, 14–27. [CrossRef]
39. Nikan, O.; Avazzadeh, Z. A locally stabilized radial basis function partition of unity technique for the sine—Gordon system in nonlinear optics. *Math. Comput. Simul.* **2022**, *199*, 394–413. [CrossRef]
40. Fasshauer, G.E. *Meshfree Approximation Methods with MATLAB*; World Scientific: Singapore, 2007; Volume 6.
41. Sarra, S.A. A local radial basis function method for advection–diffusion–reaction equations on complexly shaped domains. *Comput. Math. Appl.* **2012**, *218*, 9853–9865. [CrossRef]
42. Seydaoğlu, M. A meshless two-stage scheme for the fifth-order dispersive models in the science of waves on water. *Ocean Eng.* **2022**, *250*, 111014. [CrossRef]
43. Rasoulizadeh, M.N.; Rashidinia, J. Numerical solution for the Kawahara equation using local RBF-FD meshless method. *J. King Saud Univ. Sci.* **2020**, *32*, 2277–2283. [CrossRef]